



## City Research Online

### City, University of London Institutional Repository

---

**Citation:** Qian, K., Lan, D., Fu, F. & Li, B. (2020). Effects of Infilled Wall Opening on Load Resisting Capacity of RC Frames to Mitigate Progressive Collapse Risk. *Engineering Structures*, 223, 111196. doi: 10.1016/j.engstruct.2020.111196

This is the accepted version of the paper.

This version of the publication may differ from the final published version.

---

**Permanent repository link:** <https://openaccess.city.ac.uk/id/eprint/24679/>

**Link to published version:** <https://doi.org/10.1016/j.engstruct.2020.111196>

**Copyright:** City Research Online aims to make research outputs of City, University of London available to a wider audience. Copyright and Moral Rights remain with the author(s) and/or copyright holders. URLs from City Research Online may be freely distributed and linked to.

**Reuse:** Copies of full items can be used for personal research or study, educational, or not-for-profit purposes without prior permission or charge. Provided that the authors, title and full bibliographic details are credited, a hyperlink and/or URL is given for the original metadata page and the content is not changed in any way.

---

---

---

City Research Online:

<http://openaccess.city.ac.uk/>

[publications@city.ac.uk](mailto:publications@city.ac.uk)

---

# 1     **Effects of Infilled Wall Opening on Load Resisting Capacity of RC Frames to** 2                                    **Mitigate Progressive Collapse Risk**

3                                    Kai Qian<sup>1</sup>, Dong-Qiu Lan<sup>1</sup>, Feng Fu<sup>2</sup>, Bing Li<sup>3\*</sup>

4     <sup>1</sup>College of Civil Engineering and Architecture, Guangxi University, Nanning, China, 530004.

5     <sup>2</sup> School of Mathematics, Computer Science and Engineering, City, University of London, U.K.

6     <sup>3</sup>School of Civil and Environmental Engineering, Nanyang Technological University, Singapore  
7     639798, Singapore (corresponding author)

## 8     **ABSTRACT:**

9             To quantify the load redistribution capacity of infill walls in reinforced concrete (RC) frames  
10     to resist progressive collapse, **a series of five 1/4 scaled RC frames with or without infill walls**  
11     **were tested.** The two-bay and three-story RC frames were tested using a pushdown loading regime.  
12     It was found that the infill walls could increase the first peak load by 256 %. Even with an opening  
13     ratio of 31 %, the infill walls could still increase the first peak load by 88 %. This could be  
14     explained as the first peak load of infilled frames was attributed into equivalent struts of infill  
15     walls while the first peak load of bare frame mainly attributed in the flexural action of the beams.  
16     Beyond expectation, infill walls may not reduce the deformation capacity of the frames and  
17     secondary short struts of the infill walls could enhance the load resistance of the frame in large  
18     deformation stage. The opening ratio of 11 %, 16 %, and 31 % could decrease the first peak load  
19     of the infilled frames with solid walls by 13 %, 25 %, and 47 %, respectively. Moreover, the  
20     infilled walls with or without openings may change the position of rebar fracture of the beams.  
21     Thus, it was incorrect to simplify multi-story infilled frames into single-story substructures.

22  
23     **Keywords:** progressive collapse; reinforced concrete; infilled frame; masonry infill wall; openings

## 1. Introduction

In the event of accidental or intentional event, a building structure may suffer initial damage, such as loss of a column or partial of walls. In this context, the ability of the remaining building to develop an alternate load path to bridge initial damage has to be evaluated. Under column removal scenarios, the capacity of the alternate load path mainly depends on the beams and slabs to develop an alternative load resisting mechanism such as: a) Vierendeel Action of frame (considering the interaction of beam and column components from different stories), b) beam action (including flexural action and compressive arch action (CAA)), c) tensile catenary action (TCA) and, d) membrane action of slabs. To quantify the contribution of each mechanism, extensive experimental tests had been carried out on on-site buildings [1-5], beam-column subassemblies [6-11], beam-slab subassemblies [12-15]. Sasani *et al.* [1-5] performed several on-site tests to evaluate RC frames subjected to column removal scenarios. The test results indicated that the remaining structures only achieved elastic response as the column was actually not removed completely. And the Vierendeel action was identified as the dominant load resisting mechanism. Su *et al.* [6] tested 12 reduce-scaled beam-column subassemblies to investigate the effects of beam reinforcement ratio and span/depth ratio on the development of CAA. It was concluded that the contribution of CAA increases with decrease of span/depth ratio and beam longitudinal reinforcement ratio. Yu and Tan [7] indicated that the axial and rotational constraints at beam ends have significant effects on CAA and TCA. Yu and Tan [8] also investigated the effective of seismic detailing on enhancement of behavior of RC frames to resist progressive collapse. It was found that the benefit of seismic detailing is marginal as the resistance is dominated by either flexural or axial action. However, seismic configuration could significantly improve the behavior of RC frames against progressive collapse as increasing longitudinal reinforcement [9]. Valipour *et al.* [10] demonstrated that concrete strength has significant effects on development of CAA. Qian and Li [11] experimentally assessed the vulnerability of RC building under a corner column

1 missing scenario. It was concluded that the CAA and TCA could not be fully developed due to  
2 insufficient axial restraint at beam ends. Efforts had been paid to the quantification of the  
3 efficiency of RC slabs on enhancement of the performance of RC frames to mitigate progressive  
4 collapse [12-15], and it was found that developing compressive/tensile membrane action  
5 (CMA/TMA) in RC slabs is one of key measures. Azim *et al.* [16] had discussed critical  
6 parameters affecting load resisting mechanisms of RC beam-column or beam-slab substructures.  
7 Compared with beams and slabs, infill walls are deemed as non-structural members in  
8 conventional design and their load resistance was conservatively ignored. However, progressive  
9 collapse is a relatively low probability event and the potential resistance from secondary structural  
10 members may also reduce the vulnerability of buildings. Therefore, it was worthwhile  
11 investigating the additional progressive collapse resistance from infill walls. Up to date, little  
12 research has been done in this area. Studies [17-20] found that infill walls can provide an  
13 additional alternate load path but decreased the deformation capacity of the frames. Eren *et al.* [21]  
14 numerically investigated the effects of span/depth ratio and story height on behavior of infilled  
15 frames to resist progressive collapse. It was found that the load resistance of infilled frames was  
16 about three times higher than those counterpart bare frames. Barrosa *et al.* [22] indicated that brick  
17 infill walls could enhance the robustness of bare frames by 33 %. Xavier *et al.* [23] and Xavier [24]  
18 made numerical investigation of the effect of masonry walls on the robustness of multistory  
19 buildings under column loss scenarios. It was found that the resistance to progressive collapse  
20 relies primarily on the frame-infill interaction rather than characteristic response of the masonry  
21 wall itself subject to internal damage. Macorini and Izzuddin [25] proposed a novel modeling  
22 method for investigating the behavior of unreinforced masonry under extreme loading. Brodsky  
23 and Yankelevsky [26] tested seven infilled frames to investigate the additional load resistance of  
24 infill wall to resist progressive collapse. It was found that the masonry infill walls increased the  
25 load resistance by up to 500 %. Among the existing tests, attentions were mainly focused on solid

1 walls. Little attention was drawn to the behavior of infilled frames with openings. It was found that  
2 the load distribution behavior of infill wall with opening is distinct different from that of solid  
3 infill wall [27]. Moreover, the robustness of buildings can be enhanced significantly by walls even  
4 with gaps and openings [28]. To obtain deep understanding on opening effects, in this paper, a  
5 series of five infilled RC frames with various opening ratios were tested. The experimental results  
6 from this study could lay a foundation for the behavior of infilled frames with openings to mitigate  
7 progressive collapse and provide necessary evidence for refining existing design guidelines.

## 8 **2. Experimental program**

### 9 2.1. Design of test specimens

10 Five 1/4 scaled frames are designed and manufactured in this experimental program to study  
11 the effects of opening ratio on behavior of RC frames to mitigate progressive collapse. As shown  
12 in Table 1, one bare frame and one frame with solid infill walls are named BF and WF,  
13 respectively. Remaining three infilled frames with opening ratio of 31 %, 16 %, and 11 % are  
14 designated as WF-L, WF-M, and WF-S, respectively. The symbols of ‘L’, ‘M’, and ‘S’ represent  
15 large opening, medium opening, and small opening, respectively. The prototype building is an  
16 eight-story office building, which was designed in accordance with ACI 318-14 [29], which has  
17 span length of 7,200 mm, height of 3,600 mm in the first story and 3,300 mm in upper stories. The  
18 design live load and dead load including self-weight are 2.0 kN/m<sup>2</sup> and 6.4 kN/m<sup>2</sup>, respectively.  
19 Fig. 1 illustrates the geometry and reinforcement details of WF-L. It should be noted that the  
20 dimensions and reinforcement details of RC frames were identical. The difference was opening  
21 ratio of the infill wall. The beam span is 1800 mm and story height is 900 mm in the first floor and  
22 825 mm for the second and third floor. The cross-section of column and beam is 150 mm×150 mm  
23 and 140 mm×90 mm, respectively. The relationship between prototype frames and corresponding  
24 test models is shown in Table 2. The center column of the first story was notionally removed to  
25 simulate initial damage due to explosion or car collision. Two 400 mm × 300 mm foundations at

1 column bases were cast monolithically with column for anchorage. As shown in Fig. 1, the infill  
2 walls are reinforced with R3 as the tie-bar. The tie-bar was inserted into columns and fixed by  
3 epoxy resin. It should be noted that R6 and R3 represent plain rebar with diameter of 6 mm and 3  
4 mm, respectively. T10 rebar represents deformed rebar with diameter of 10 mm. Fig. 2 shows the  
5 typical dimensions and opening details of rest specimens.

## 6 **2.2. Material properties**

7 At the day of testing, average cylinder compressive strengths of concrete were measured as 32  
8 MPa, 34 MPa, 31 MPa, 31 MPa, and 32 MPa for Specimens BF, WF, WF-S, WF-M, and WF-L,  
9 respectively. The compressive strength of the masonry was 17.3 MPa. The measured compressive  
10 strength of mortar was 16.5 MPa. For the masonry unit (combination of brick and mortar), the  
11 measured compressive strength and shear strength were 10.5 MPa and 1.1 MPa, respectively.  
12 Moreover, the properties of reinforcements are shown in Table 3.

## 13 **2.3 Test setup and instrumentations**

14 Figs. 3 and 4 show the test setup and the instrumentations layout, respectively. As illustrated  
15 in Fig. 3, the column bases of the specimens are fixed to the strong floor through the enlarged  
16 foundations. The ground center column was removed in advance and a hydraulic jack with stroke  
17 of 600 mm was utilized to apply a concentrated load at the top of center column. Displacement-  
18 controlled method was adopted for this load application. Before reaching first peak load of each  
19 specimen, 1 mm increment was selected. After that stage, displacement increment of 5 mm was  
20 adopted. To prevent out-of-plane failure of the specimen, a steel column and a steel assembly are  
21 specially designed. To simulate horizontal restraints from the beams in surrounding bays,  
22 overhanging beams were connected with the A-frame by three rollers. In addition, to measure the  
23 axial force, tension/compression load cell was installed for each roller. As illustrated in Fig. 4, a  
24 series of linear variable deformation transducers (LVDTs) were installed beneath the beam in the  
25 first floor to measure the deformation shape of the beams. A series of LVDTs are also installed

1 along the column height and joints to measure the lateral displacements of the columns and shear  
2 deformation of the joints.

### 3 **3. Experimental results**

#### 4 3.1. Global behavior

5 *Specimen BF*: The crack pattern of the bare frame BF at center column displacement (CCD)  
6 of 50 mm is illustrated in Fig. 5a. Actually, the first crack was observed at beam end nearby the  
7 center column (BENC) at a CCD of 10 mm. When CCD increased to 23 mm, crack also formed at  
8 the cut-off points of the top beam longitudinal rebar. The cracks occurred much earlier in the first  
9 and second floor than in the third one. When CCD reached 280 mm, **diagonal shear crack** occurred  
10 at the exterior joint in the first floor. However, no shear cracks occurred at the interior joints until  
11 failure. **The maximum width of the shear crack in the exterior joint of first story reached 8 mm**  
12 when CCD reached 358 mm. The load resistance versus vertical CCD of BF is shown in Fig. 6.  
13 The yield load (YL) of 28 kN is measured at CCD of 21 mm. However, the first peak load (FPL)  
14 of 32 kN was obtained at a CCD of 38 mm, which is about 114 % of that of YL. Different from  
15 conventional reinforced concrete (RC) frames with simplified fixed boundary conditions at beam  
16 ends [7-9], the benefits of CAA **are** not obvious, which is mainly due to less horizontal constraints  
17 from exterior joints. Re-ascending was observed when CCD reached 153 mm due to mobilization  
18 of TCA. The ultimate load (UL) of 29 kN was measured at a CCD of 298 mm. At this  
19 displacement stage, rebar fracture occurred at the cut-off points. Further increasing the  
20 displacement, bottom rebar at BENC and top rebar at cut-off points fractured successively. Fig. 7  
21 illustrates the failure mode of BF. As shown in the figure, bottom rebar was fractured at BENC  
22 while top rebar was fractured at cut-off points. No shear cracks were observed in the interior joints  
23 but severe shear cracks were noticed in the exterior joint in the first floor, similar to previous full-  
24 scale joint tests to resist progressive collapse [30-31].

1            **Specimen WF-L:** Fig. 5b shows the crack pattern of WF-L at a CCD of 50 mm. Different  
2 from BF, the first crack was observed in infilled wall at a CCD of 6 mm. Further increasing CCD  
3 to 8 mm, flexural cracks were also formed at the cut-off points of the beam top longitudinal rebar.  
4 When the CCD increased to 21 mm, detachment was observed in the middle part of the wall  
5 between two openings. With further increasing CCD, more cracks formed in the beams. Moreover,  
6 horizontal cracks occurred at the lower part of the infilled wall (below the openings). As the  
7 opening was so large, no direct diagonal crack was formed in the walls. In other words, no main  
8 diagonal strut could be formed for each panel of the wall. As shown in Fig. 6, at a CCD of 9 mm,  
9 the FPL of 60 kN, which was 188 % of that of BF, was measured. Although the load resistance  
10 began to drop after CCD of 14 mm, the load resistance began to re-ascend after CCD of 203 mm,  
11 which was attributed into the mobilization of TCA in beam longitudinal reinforcement. Thus, the  
12 infill walls with relatively large opening will not prevent the development of TCA. The UL of 40  
13 kN was measured at CCD of 380 mm. The failure mode of WF-L is shown in Fig. 8. **It can be seen**  
14 **that the middle wall panel in the second story almost detached to the beams completely.** Evident  
15 slippage was observed in the wall pier in the third story. Moreover, **the lower part of the wall**  
16 **(below the openings) deformed together with the beam, acting as a deep beam.** Rebar fracture was  
17 observed in the beams from the second story to the third story in sequence. However, it should be  
18 noted that the fracture of beam top rebar is further away from the side column when the beams  
19 located from the first story to third one. To the contrary, the fracture of beam bottom rebar is closer  
20 to the center column when the beams located from the first story to the third story. **Shear crack**  
21 **with maximum width of 3.8 mm was measured at exterior joint of first story.**

22            **Specimen WF-M:** Similar to WF-L, the first crack was observed in the infill wall of WF-M  
23 at a CCD of 5 mm. Different from WF-L, the first crack in WF-M is diagonal stepped. When CCD  
24 reached 15 mm, cracks were also observed in the beams. At this displacement stage, bed joint  
25 slippage was observed in the wall connected with the beam in the second story. Further increasing

1 CCD, the diagonal stepped cracks in the middle wall pier become much wider and horizontal  
2 cracks developed in the lower continual part of the wall. Fig. 5c gives the crack pattern of WF-M  
3 at a CCD of 50 mm. As shown in Fig. 6, when CCD reached 7 mm, the FPL of 85 kN, which is  
4 266 % of that of BF, was measured. When the CCD increased to 122 mm, the decrease of load  
5 resistance became milder. However, the load resistance re-ascending was observed when CCD was  
6 larger than 182 mm, due to the mobilization of TCA. When CCD further increased to 399 mm, the  
7 UL of 48 kN, which was about 56 % of its FPL, is obtained. Fig. 9 shows the failure mode of WF-  
8 M. Compared to WF-L, main diagonal stepped crack was formed at the middle wall pier, rather  
9 than horizontal crack and detachment. Moreover, although severe damage occurred in infill wall,  
10 the integrity of the walls in WF-M is greater than that in WF-L. Although rebar fracture was  
11 observed in the top longitudinal rebar in third story, the damage of the beams is much milder than  
12 that in WF-L. Shear crack with maximum width of 6.2 mm was measured at exterior joint of first  
13 story.

14 **Specimen WF-S:** The first crack in infill wall of WF-S was observed at a CCD of 3 mm,  
15 which was much earlier than that of WF-M and WF-L. Similar to WF-M, the first crack is  
16 observed in the middle wall pier and it is diagonal, rather than horizontal. At a CCD of 6 mm, the  
17 FPL of 99 kN, which was 309 % of that of BF, was obtained. Further increasing the CCD to 21  
18 mm, the bed joint slippage was observed in infill wall. Further increasing the CCD, the diagonal  
19 stepped cracks became much wider. Fig. 5d illustrates the crack pattern of WF-S at CCD of 50 mm.  
20 As shown in Fig. 6, after CCD of 21 mm, the load resistance of the specimen began to drop. At  
21 CCD of 198 mm, re-ascending was observed. The UL of 54 kN, which was about 186 % of that of  
22 BF. The failure mode of WF-S is shown in Fig. 10. As shown in the figure, the integrity of infill  
23 wall in WF-S is worse than that of WF-M, which is unexpected. Different to WF-M, severe  
24 detachment was observed in middle wall panel. Rebar fracture was occurred in all beams. Shear  
25 crack with maximum width of 2.1 mm was measured at exterior joint of first story.

1

2        *Specimen WF*: Fig. 5e illustrates the crack pattern of WF at a CCD of 50 mm. As shown in

3 Fig. 6, first crack was observed in the infilled wall at a CCD of 1 mm, which was much earlier than

4 the wall with openings. The crack in RC beam was first observed at a CCD of 2 mm. Further

5 increasing CCD to 3 mm, more cracks were formed in infill walls. The FPL of 114 kN was

6 achieved at this loading stage. Moreover, flexural cracks formed in the beams. Different from BF,

7 the cracks were not always formed at the BNEC and cut-off points. Actually, the position of

8 flexural crack is quite different. Based on crack width observations, the main load resisting

9 mechanism at FPL stage was compressive strut of the infill walls (strain gauge results confirmed

10 this conclusion). When CCD reached 10 mm, bed joints slippage was observed in infilled walls

11 and the load resistance dropped significantly. With further increasing CCD, the bed joints slippage

12 become more severe. However, it should be noted that the bed joint slippage in the second story

13 was much earlier and more severe than that in the third story. The load resistance of the specimen

14 kept almost constant when the CCD reached 51 mm. After that, the main diagonal strut had lost its

15 load resistance and several secondary compressive struts beyond the center zone kicked in. Further

16 increasing CCD, more severe slippage of the bed joint was observed. Some of the bricks were even

17 fully detached. When CCD reached 292 mm, rebar was fractured from the first story to the third

18 story successively. Fig. 11 shows the failure mode of WF. The main diagonal stepped crack

19 become very wide and some of bed joints were fully detached. Different to BF, diagonal shear

20 crack was also observed in exterior joint in the second story. Moreover, although rebar fracture

21 was observed in the beams in all stories, the position of rebar fracture was quite different with that

22 of BF. In general, the integrity of infill walls is best in WF. Shear crack with maximum width of

23 7.6 mm was measured at exterior joint of first story.

### 3.2. Deflection shape of the beams in the first floor

Fig. 12 illustrates the deflection shape of beams in the first floor of BF and WF-L in accordance with different stages. For BF, as shown in the Fig. 12a, from the beginning of the test, the slope of the beam near the edge column is obviously less than that near to the center column. At final stage of the test, the chord rotation, which is defined as the ratio of CCD to the beam clear span, coincides with the slope of the beam near to the center column but overestimates the slope of the beam near to the edge column. As shown in the Fig. 12b, double curvature was observed for beam deformation of WF-L. The relatively milder slope of the beam near to the center column can be attributed into the composite action of infill walls and beams. At final stage of test, converse to BF, the chord rotation will overestimate the rotation of beam section near to the center column but underestimate the rotation of the beam section near to the side column. It should be noted that the deformation shape of the beam in the first story of WF-M, WF-S, and WF is quite similar to that of WF-L.

### 3.3. Horizontal movement of exterior joints

As mentioned above, a series of LVDTs were installed horizontally to measure the lateral movement of exterior joints during test. The horizontal movements of exterior joints versus CCD relationships were given in Fig. 13. For BF, the maximum outward movement of -10 mm was measured in the third floor at CCD of 110 mm. When CCD reached about 233 mm, exterior joints moved back to their original position. The maximum inward movement of 54 mm was measured in the third floor at CCD of 370 mm. For WF-L, similar to BF, the maximum outward movement of -12 mm and inward movement of 53 mm were measured at exterior joint in the third floor. The larger outward movement was mainly due to infill walls working as a compressive strut, which bring in additional outward movement. The maximum outward movement of WF-M, WF-S, and WF was -13 mm, -14 mm, and -16 mm, respectively. It was confirmed with the failure modes and load-displacement curve: the larger the openings, the less efficiency of equivalent compressive

1 strut. Moreover, the maximum inward movement of WF-M, WF-S, and WF was 50 mm, 48 mm,  
2 and 47 mm, respectively. The less inward movement of WF in large deformation stage was mainly  
3 attributed into equivalent compressive strut could provide additional horizontal constraints when  
4 TCA was mobilized in beams.

#### 5 3.4. Strain gauge readings

6 To investigate the resistance mechanism of frames during the test process, a series of strain  
7 gauges were glued symmetrically at longitudinal reinforcements of the second and third floor beam,  
8 as shown in Fig.1. Fig. 14 gives the variation of strain gauge results. As shown in Fig.14a, for top  
9 reinforcement of BF, the maximum tensile strain was measured at a distance of 435 mm from the  
10 interface of side column for both second and third stories. When TCA mobilized, the compressive  
11 strain in the beam end near to the center column began to reduce. However, even at final stage of  
12 test, compressive strain still observed in the beam end near to the center column. As shown in Fig.  
13 14b, the maximum tensile strain in the bottom reinforcement of BF was measured at the interface  
14 of center column for both stories. In addition, when TCA began to develop, the tensile strain of  
15 bottom reinforcement continued to increase. Thus, it was demonstrated that both top and bottom  
16 reinforcement contributed to TCA. Finally, from strain gauge results of BF, it was concluded that a  
17 single-story substructure could well represent the behavior of bare planar 2D multi-story frame.  
18 For top reinforcement of WF-L, the maximum tensile strain was measured at different position for  
19 second and third floor, which agree with the crack pattern of the specimen well. Moreover,  
20 different to BF, the measured maximum tensile strain of the bottom rebar was also quite different  
21 to those of the second and third floors. Moreover, when CCD increased to 184 mm, tensile strain  
22 was further increased significantly with further increase of the CCD. Therefore, TCA could  
23 develop in infilled frames with openings, which agrees with the horizontal movement of joints well.  
24 For WF-M, WF-S, and WF, similar trends were observed although the position of maximum  
25 tensile strain may be different.

### 1 3.5. Shear rotation in exterior joints

2 To monitor the behavior of joint panels, two LVDTs were installed orthogonally at side  
3 joints (Item 7 in Fig. 3). Fig. 15 provides methods to determine the shear distortion of the joints.  
4 As shown in the figure, the joint shear distortion  $\gamma$  can be converted from the readings of two  
5 LVDTs. It is worth pointing out that  $\Delta_1$  and  $\Delta_2$  are stretch deformation and shorten deformation  
6 of two LVDTs, respectively; and  $a$  is length of square joint panel. Figs. 16-18 illustrate the  
7 variation of shear panel of joints in different stories of different specimens. As shown in Fig. 16a,  
8 before CCD reached 183 mm, the maximum distortion of  $-14 \times 10^{-4}$  rad was measured in exterior  
9 joint of first story. The negative value means the shear distortion opposite to the one shown in Fig.  
10 15. When CCD exceeded 183 mm, the negative distortion began to decrease due to TCA that  
11 developed in the beams, which is prone to pulling the joint inward. The maximum distortion of  
12  $225 \times 10^{-4}$  rad was measured in exterior joint in the first story at the final of test. Regarding the  
13 exterior joints in the second and third stories, the maximum distortion was  $13 \times 10^{-4}$  rad and  $10 \times 10^{-4}$   
14 rad, respectively. For interior joints, as shown in Fig. 16b, the maximum negative and positive  
15 shear distortion were ranged from  $-2 \times 10^{-4}$  rad to  $1 \times 10^{-4}$  rad. Less distortion in interior joints was  
16 mainly due to overhanging beams could provide horizontal reaction force, which significantly  
17 reduced the shear force in the joints. As shown in Figs. 17a and 18a, the maximum negative shear  
18 distortion in exterior joints of WF-L and WF was  $-7 \times 10^{-4}$  rad and  $-9 \times 10^{-4}$  rad, respectively.  
19 However, the maximum positive shear distortion in interior joints of WF-L and WF was  $30 \times 10^{-4}$   
20 rad and  $57 \times 10^{-4}$  rad, respectively. Thus, the infill walls even with large opening ratio could  
21 decrease the shear distortion of the exterior joints significantly. However, it should be noted that  
22 the maximum shear distortion of WF-L was measured in the second floor while the one of WF was  
23 measured in the first floor. This was mainly due to the interaction between the infill wall and  
24 surrounding frames, which was very complicated.

### 25 4. Results analysis and discussion

#### 4.1. Discussion of the effects of infill walls and openings

Comparing the FPL of WF and BF, solid infill wall could increase the FPL and UL by 256 % and 100 %, respectively. The increasing of the FPL was mainly due to diagonal struts that formed in the walls (refer to Fig. 20a). In large deformation stage, greater UL measured in WF could be attributed into secondary struts formed in relatively intact walls (refer to Fig. 20b). Comparing Figs. 7 and 11, the interaction between the solid walls and surrounding frame could change the position of rebar fracture. The opening ratio of WF-L, WF-M, and WF-S is 31 %, 16 %, and 11 %, respectively. The FPL of WF-L, WF-M, WF-S, and WF were 60 kN, 85 kN, 99 kN, and 114 kN, respectively. Therefore, the opening ratio of 31 %, 16 %, and 11 % decreased the FPL of WF by 47 %, 25 %, and 13 %, respectively. The disadvantage effects of openings on FPL were mainly due to the openings weakening to the load redistribution capacity of compressive struts of infill wall. As shown in Fig. 5, for WF-L, which has opening ratio of 31 %, no diagonal compressive strut was formed in infill wall. For WF-M, which has opening ratio of 16 %, diagonal compressive strut was only formed in the middle pier between the openings. However, for WF-S, which has opening ratio of 11 %, struts could be formed diagonally, which are similar to that of WF.

The UL of WF-L, WF-M, WF-S, and WF were 40 kN, 48 kN, 54 kN, and 58 kN, respectively. Therefore, the opening ratio of 31 %, 16 %, and 11 % decreased the UL of WF by 31 %, 17 %, and 7 %, respectively. As the contribution of TCA of RC beam on UL was similar, the detrimental effects of openings on UL were mainly due to openings weakening of the secondary struts. Considering the complexity of stress distribution in infill walls with openings, numerical analysis could be adopted for accurate determination of the struts. Moreover, as mentioned above, the first crack was formed in infill walls of WF, WF-S, WF-M, and WF-L at CCD of 1 mm, 3 mm, 5 mm, and 8 mm. Thus, the opening ratio may decrease the stiffness of the walls and delay the formation of cracks in the walls. Moreover, as shown in Figs. 8 to 10, the opening ratio may reduce the integrity of the walls in large deformation stage, especially for the

1 opening ratio reached 31 %. The maximum width of the shear crack in the exterior joint of first  
2 story of BF, WF-L, WF-M, WF-S, and WF was 8.0 mm, 3.8 mm, 6.2 mm, 2.1 mm, and 7.6 mm,  
3 respectively. Comparing the failure mode of these specimens, it was found that the crack width of  
4 exterior joint was controlled by the efficiency of secondary struts. For WF-M, the width of intact  
5 wall panel nearby the exterior side column was less than WF-L and WF-S, which reduced the  
6 efficiency of secondary strut. For WF, unexpected detachment was observed between the wall  
7 panel and exterior side column at large deformation stage, which may prevent the development of  
8 secondary struts. Furthermore, the deformation capacity of BF, WF-L, WF-M, WF-S, and WF was  
9 370 mm, 380 mm, 399 mm, 431 mm, and 393 mm, respectively. Fortunately, the infill walls and  
10 openings may not reduce the deformation capacity of the frames. Therefore, it was convinced to  
11 consider the contribution of infill walls in evaluation of the load redistribution capacity of RC  
12 frames, as progressive collapse incidents actually are low-possibility events.

#### 13 4.2. De-composition of the load resistance

14 To quantify the contribution of infill walls to resist progressive collapse, the load resistance  
15 of infilled frames was de-composited by subtracting the load resistance of infilled frames by that of  
16 bare frame at same displacement. As shown in Fig. 19, initially, 82 % of the load resistance of  
17 WF-L from infill wall. At a CCD of 14 mm or at stage of FPL, 61 % of the load resistance was  
18 attributed into the infill wall with opening ratio of 31 %. Further increasing the CCD, the  
19 contribution of infill wall dropped to 40 %. After that, the percentage kept decreasing until CCD of  
20 204 mm. At this stage, the contribution of infill wall only 7 %. This could be explained by the  
21 mobilization of TCA in RC beams. Then, the contribution of infill wall kept re-ascending due to  
22 fracture of rebar successively, which reduced the load resistance from TCA. At the final of test, the  
23 contribution of infill wall was about 60 % although the infill wall has opening ratio of 31 %. Thus,  
24 even in large deformation stage, the load resistance of infill wall could not be ignored. For WF-M,  
25 initially, 87 % of the load resistance was attributed by the infill wall. At stage of FPL, 81 % of the

1 load resistance was attributed by the infill wall. Then, with increasing CCD, the contribution of  
 2 infill wall kept to decreasing until CCD of 264 mm. The minimum percentage of infill wall was  
 3 22 %. Similar to WF-L, increasing contribution of infill wall was observed when further increase  
 4 of CCD. The contribution of infill wall was about 70 % at final of test. For WF-S and WF, over 90 %  
 5 of the load resistance was attributed by the infill wall initially. The minimum contribution of infill  
 6 wall was 35 % and 43 % for WF-S and WF, respectively. Thus, comparing to the walls with  
 7 opening ratio of 31 %, the wall with opening ratio of 11 % and solid infill wall could provide  
 8 larger additional load resistance in large deformation stage.

#### 9 4.3. Dynamic response of tested specimens

10 Although the opening effects on quasi-static response of RC frames to resist progressive  
 11 collapse had been quantified, the opening effects on dynamic load resisting capacity of the frames  
 12 still need investigation. Therefore, it was necessary to evaluate the effects of opening on dynamic  
 13 response of tested specimens. Izzuddin *et al.* [32] proposed energy-based method was adopted in  
 14 this dynamic capacity evaluation (refer to Eq. 1).

$$P_d(u_d) = \frac{1}{u_d} \int_0^{u_d} P_{NS}(u) du \quad (1)$$

15 where  $P_d(u)$  and  $P_{NS}(u)$  are the dynamic load resistance and static load resistance estimated at the  
 16 displacement demand  $u$ , respectively.

17 As given in Fig. 21, the dynamic peak load of BF, WF-L, WF-M, WF-S, and WF were 27  
 18 kN, 55 kN, 80 kN, 86 kN, and 97 kN, respectively. Therefore, the solid infill wall increased the  
 19 dynamic peak load by 259 %. The opening ratio of 31 %, 16 %, and 11 % decreased the dynamic  
 20 peak load of WF by 43 %, 18 %, and 11 %, respectively. Comparing to the detrimental effects on  
 21 static peak load, the opening effects on dynamic peak load were milder.

## 22 6. Conclusions

23 Based on experimental results and numerical analysis, the conclusions were drawn:

- 1 1. For bare frames, in the initial stage, the flexural action provides the load resistance.  
2 Compressive arch action was ineffective as the external joints controlled the extent of the  
3 horizontal constraints for the beam ends. For infilled frames with or without openings, in initial  
4 stage, the equivalent compressive strut of infilled walls provided majority of the load resistance.  
5 However, in large deformation stage, the load resistance of both bare frame and infilled frames  
6 mainly relied on tensile catenary action developed in the beams. However, as the secondary  
7 compressive struts could provide additional load redistribution path for infilled frames even in  
8 large deformation stage, the ultimate load capacity of infilled frames was also greater than that  
9 of bare frames.
- 10 2. Comparing the failure mode of bare frames and infilled frames, it was found that infill walls  
11 may change the failure mode of the bare frame significantly. The position of plastic hinge and  
12 rebar fracture in infilled frames was different in different story. Therefore, for infilled frames,  
13 it was not reliable to simplify the multi-story frame into single story beam-column  
14 substructures. Conversely, for bare frames, the failure mode of each floor was similar. Based  
15 on the measured shear distortion of exterior joints, infill walls have benefits towards reducing  
16 the shear distortion of the joints.
- 17 3. Comparing to bare frame, the solid infill walls increased the first peak load and ultimate load  
18 by 256 % and 100 %, respectively. Moreover, the ultimate deformation capacity of the bare  
19 frame and infilled frames with solid walls was 370 mm and 393 mm, respectively. Thus, solid  
20 walls will not reduce the deformation capacity.
- 21 4. The opening ratio of 31 %, 16 %, and 11 % will decrease the static peak load of the infilled  
22 frames with solid walls by 47 %, 25 %, and 13 %, respectively. However, the opening ratio of  
23 31 %, 16 %, and 11 % will decrease the dynamic peak load by 43 %, 18 %, and 11 %, respectively.  
24 Therefore, the detrimental effects of the openings are similar for static and  
25 ultimate load resistance.

## 1 **Future works**

2 To understand the effects of span/depth ratio on behavior of infilled frames to mitigate  
3 progressive collapse, more tests should be carried out in the future.

## 4 **Acknowledgements**

5 The authors gratefully acknowledge the financial support provided by the Natural Science  
6 Foundation of China (Nos. 51778153, 51568004, 51478118). The high-level innovation team in  
7 colleges and universities and excellence scholar program in Guangxi (201738). Any opinions,  
8 findings and conclusions expressed in this paper do not necessary reflect the view of Natural  
9 Science Foundation of China.

## 10 **References**

- 11 [1] Sasani M, Bazan M, Sagioglu S. Experimental and analytical progressive collapse evaluation  
12 of actual reinforced concrete structure. *ACI Structural J.* 2007; 104(6):731-39.
- 13 [2] Sasani M. Response of a reinforced concrete infilled-frame structure to removal of two  
14 adjacent columns. *Eng Struct.* 2008; 30(9):2478-91.
- 15 [3] Sasani M, Sagioglu S. Progressive collapse resistance of hotel San Diego. *J. Struct Eng.*  
16 2008; 134(9): 478-88.
- 17 [4] Sasani M, Sagioglu S. Gravity load redistribution and progressive collapse resistance of 20-  
18 story reinforced concrete structure following loss of interior column. *ACI Struct J.* 2010; 107  
19 (6):636-645.
- 20 [5] Sasani M, Kazemi A, Sagioglu S, Forest S. Progressive collapse resistance of an actual 11-  
21 story structure subjected to severe initial damage. *J. Struct Eng.* 2011; 137(9): 893-902.
- 22 [6] Su YP, Tian Y, Song XS. Progressive collapse resistance of axially-restrained frame beams.  
23 *ACI Struct J.* 2009; 106(5): 600-7.
- 24 [7] Yu J, Tan KH. Structural behavior of rc beam-column subassemblages under a middle column  
25 removal scenario. *J. Struct Eng.* 2013; 139(2): 233-50.
- 26 [8] Yu J, Tan KH. Experimental and numerical investigation on progressive collapse resistance of  
27 reinforced concrete beam column sub-assemblages. *Eng Struct.* 2013; 55: 90-106.

- 1 [9] Kim J, Choi H. The monotonic loading tests of RC beam-column subassemblage strengthened  
2 to prevent progressive collapse. *International Journal of Concrete Structures and Materials*  
3 2016; 9(4):401-13
- 4 [10] Valipour H, Vessali N, Foster SJ, Samali B. Influence of concrete compressive strength on the  
5 arching behaviour of reinforced concrete beam assemblages. *Adv. Struct. Eng.* 2015;  
6 18(8):1199-214.
- 7 [11] Qian K, Li B. Dynamic performance of RC beam-column substructures under the scenario of  
8 the loss of a corner column-experimental results. *Eng. Struct.* 2012; 42:154-67.
- 9 [12] Parasad S, Hutchinson TC. Evaluation of older reinforced concrete floor slabs under corner  
10 support failure. *ACI Struct. J.* 2014; 111(4): 839-49.
- 11 [13] Qian K, Li B, Ma JX. Load-carrying mechanism to resist progressive collapse of RC buildings.  
12 *J Struct. Eng.* 2015; 141(2):4016407.
- 13 [14] Qian K, Li B. Strengthening of multibay reinforced concrete flat slabs to mitigate progressive  
14 collapse. *J. Struct. Eng.* 2015; 141(6):04014154.
- 15 [15] Qian K, Li B. Strengthening and retrofitting precast concrete buildings to mitigate progressive  
16 collapse using externally bonded GFRP strips. *J. Compos. Const.* 2019; 23(3): 4019018.
- 17 [16] Azim I, Yang J, Bhatta S, Wang F, Liu QF. Factors influencing the progressive collapse  
18 resistance of RC frame structures. *Journal of Building Engineering* 2020; 27.
- 19 [17] Li S, Shan SD, Zhai CH, Xie LL. Experimental and numerical study on progressive collapse  
20 process of RC frames with full-height infill walls. *Engineering Failure Analysis* 2016;  
21 59:57–68.
- 22 [18] Qian K, Li B. Effects of masonry infill wall on the performance of RC frames to resist  
23 progressive collapse. *J. Struct. Eng.* 2017; 143(9): 04017118.
- 24 [19] Baghi H, Oliveira A, Valença J, Cavaco E, Neves L, Júlio E. Behavior of reinforced concrete  
25 frame with masonry infill wall subjected to vertical load. *Eng. Struct.* 2018; 171(15):476-87.
- 26 [20] Tsai MH, Huang TC. Numerical investigation on the progressive collapse resistance of an RC  
27 building with brick infills under column loss. *International Journal of Civil and*  
28 *Environmental Engineering* 2011; 5(10): 483–90.
- 29 [21] Eren N, Brunesi E, Nascimbene R. Influence of masonry infills on the progressive collapse  
30 resistance of reinforced concrete framed buildings. *Eng. Struct.* 2019; 178(1):375-94.
- 31 [22] Barrosa M, Cavacob E, Nevesc L, Júliod E. Effect of non-structural masonry brick infill walls  
32 on the robustness of a RC framed building severely damaged due to a landslide. *Eng. Struct.*  
33 2019; 180(1):274-83.

- 1 [23]Xavier FB, Macorini L, Izzuddin BA. Robustness of multistory buildings with masonry infill.  
2 *J. Perform. Constr. Facil.* 2015; B4014004.
- 3 [24]Xavier FB. The role of masonry infill in progressive collapse mitigation of multi-storey  
4 buildings. PhD dissertation, Imperial College London, London; 2015.
- 5 [25]Macorini L, Izzuddin BA. Nonlinear analysis of unreinforced masonry walls under blast  
6 loading using mesoscale partitioned modeling. *J. Struct. Eng.* 2014; 140(8): A4014002.
- 7 [26]Brodsky A, Yankelevsky DZ. Resistance of reinforced concrete frames with masonry infill  
8 walls to in-plane gravity loading due to loss of a supporting column. *Eng. Struct.* 2017;  
9 140:134-50.
- 10 [27]Shan SD, Li S, Xu SY, Xie LL. Experimental study on the progressive collapse performance  
11 of RC frames with infill walls. *Eng. Struct.* 2016; 111: 80-92.
- 12 [28]Xavier FB, Macorini L, Izzuddin BA, Chisari C, Gattesco N, Noe S, Amadio C. Pushdown  
13 tests on masonry infilled frames for assessment of building robustness. *J. Struct Eng.* 2017;  
14 143 (9): 04017088.
- 15 [29]ACI Committee 318. Building code requirements for structural concrete (ACI 318-14) and  
16 commentary. American Concrete Institute, Farmington Hills, MI, 503 pp; 2014.
- 17 [30]Qian K, Li B. Experimental and analytical assessment on RC interior beam-column  
18 subassemblages for progressive collapse. *J. Perform. Constr. Facil.* 2012; 26(5) 576-89.
- 19 [31]Yap SL, Li B. Experimental investigation of RC exterior beam-column subassemblages for  
20 progressive collapse. *ACI Struct J.* 2011; 108(5): 542–52.
- 21 [32]Izzuddin BA, Vlassis AG, Elghazouli AY, Nethercot DA. Progressive collapse of multi-storey  
22 buildings due to sudden column loss—Part I: Simplified assessment framework. *Eng. Struct.*  
23 2008; 30(5):1309-18.

## TABLES AND FIGURES

1  
2  
3  
4  
5  
6  
7  
8  
9  
10  
11  
12  
13  
14  
15  
16  
17  
18  
19  
20  
21  
22  
23  
24  
25  
26  
27  
28  
29  
30  
31  
32  
33

### List of Tables:

**Table 1-** Specimen properties

**Table 2-** Relationship between prototype frames and corresponding test specimens

**Table 3-** Reinforcements properties

**Table 4-** Test results

### List of Figures:

**Fig. 1** Dimension and reinforcement details of Specimen WF-L: (a) elevation view; (b) cross sections

**Fig. 2** Design details of opening specimens: (a) WF-M; (b) WF-S

**Fig. 3** Overview of WF-M in position ready for testing

**Fig. 4** Schematic view of test setup and instrumentation layout

**Fig. 5** Crack pattern of the specimens at the CCD of 50 mm: (a) BF; (b) WF-L; (c) WF-M; (d) WF-S; (e) WF

**Fig. 6** Load resistance versus vertical displacement at center column

**Fig. 7** Failure mode of BF

**Fig. 8** Failure mode of WF-L

**Fig. 9** Failure mode of WF-M

**Fig. 10** Failure mode of WF-S

**Fig. 11** Failure mode of WF

**Fig. 12** Overall deflection curve of beams in the first story: (a) BF, (b) WF-L

**Fig. 13** Horizontal movement of the exterior joints at different storey: (a) BF; (b) WF-M; (c) WF-S; (d) WF

**Fig. 14** Variation of strain results along the third floor beam longitudinal reinforcements: (a) top rebar in BF; (b) bottom rebar in BF; (c) top rebar in WF-L; (d) bottom rebar in WF-L; (e) top rebar in WF-S; (f) bottom rebar in WF-S; (g) top rebar in WF; (h) bottom rebar in WF

**Fig. 15** Method to determine the distortion of shear panel in joints

**Fig. 16** Variation of shear panel distortions of the joints in different stories of BF: (a) exterior joints; (b) interior joint

**Fig. 17** Variation of shear panel distortions of the joints in different stories of WF-L: (a) exterior joints; (b) interior joint

1 **Fig. 18** Variation of shear panel distortions of the joints in different stories of WF: (a) exterior  
 2 joints; (b) interior joint

3 **Fig. 19** De-composition of the load resistance from RC frames and infill walls: (a) WF-L, (b) WF-  
 4 M, (c) WF-S, and (d) WF

5 **Fig. 20** Dynamic performance of the specimens

6  
 7 **Table 1**-Specimen properties

Specimen	Beam longitudinal reinforcement				Characteristic and Opening Size	Opening Rate
	Middle Span		Beam Ends			
	Top	Bottom	Top	Bottom		
BF	2R6	3R6	4R6	2R6	Bare frame	100 %
WF-L	2R6	3R6	4R6	2R6	400 mm × 440 mm	31 %
WF-M	2R6	3R6	4R6	2R6	300 mm × 300 mm	16 %
WF-S	2R6	3R6	4R6	2R6	250 mm × 250 mm	11 %
WF	2R6	3R6	4R6	2R6	solid wall	0

8 Note: R6 represents plain bar of with diameter of 6 mm.

9  
 10 **Table 2**-Relationship between prototype frames and corresponding test models

Items	Prototype frame	Test model
Column size	Depth	150 mm
	Width	150 mm
Beam size	Depth	140 mm
	Width	90 mm
Story Height	First Story	900 mm
	Upper Story	825 mm
Concrete Cover	Beam	7 mm
	Rebar ratio	10 mm

11  
 12 Note: T = deform reinforcing bar; R = plain reinforcing bar.

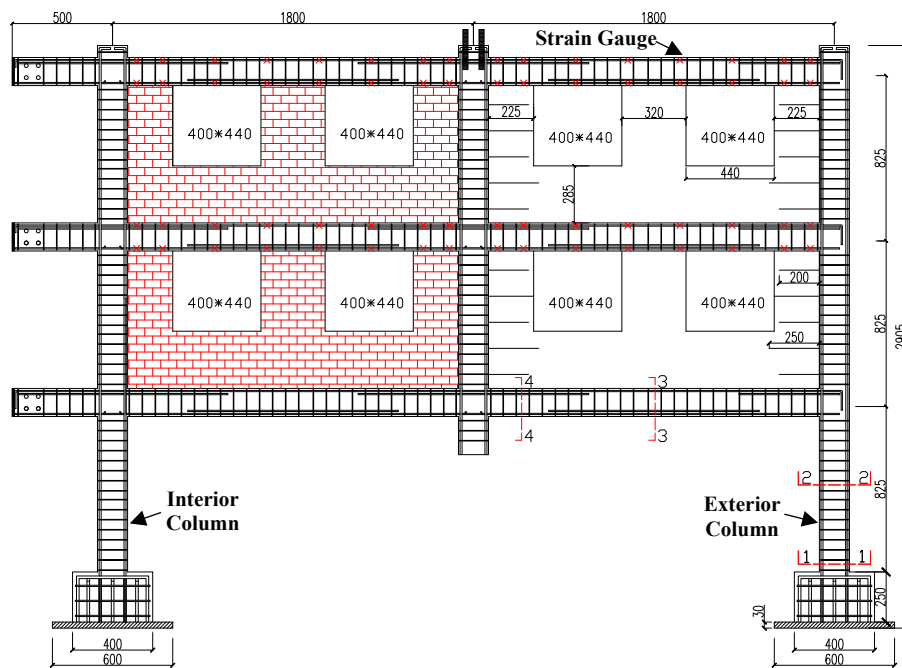
13  
 14  
 15  
 16  
 17 **Table 3**-Reinforcements properties

Items	Nominal diameter	Yield strength	Ultimate strength	Elongation
T10	10 mm	515 MPa	594 MPa	16.9 %
R6	6 mm	449 MPa	537 MPa	13.3 %
R3	3 mm	417 MPa	479 MPa	9.7 %

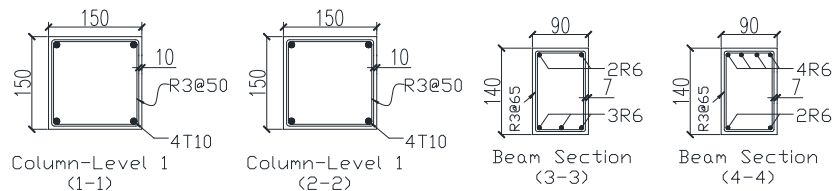
18  
 19  
 20  
 21  
 22  
 23 **Table 4**- Test results

Specimen ID	Critical Load (kN)		Critical Displacement (mm)		Deformation Capacity (mm)
	FPL	UL	FPL	UL	
BF	32	29	38	298	370
WF-L	60	40	14	380	380
WF-M	85	48	7	399	399
WF-S	99	54	6	420	431
WF	114	58	3	299	393

Note: FPL means first peak load capacity; UL represents ultimate load capacity.



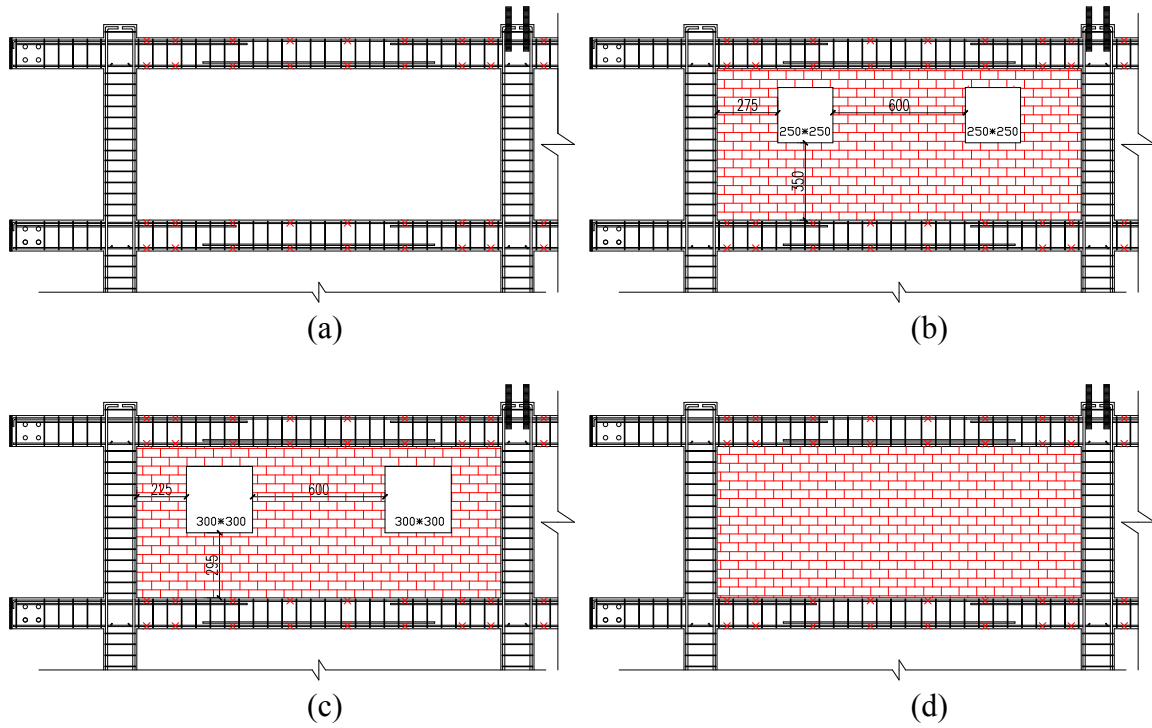
(a)



(b)

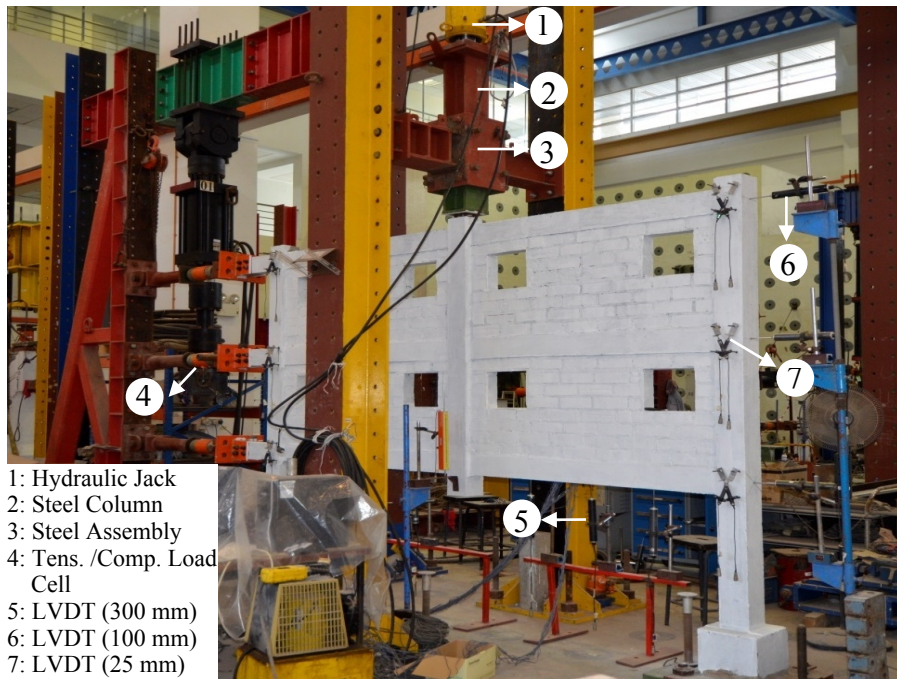
**Fig. 1** Dimension and reinforcement details of Specimen WF-L: (a) elevation view; (b) cross sections (Note: unit in mm)

1  
2  
3



4  
5  
6  
7  
8  
9

**Fig. 2** Design details of opening specimens: (a) BF, (b) WF-S, (c) WF-M, and (d) WF  
Note: unit in mm



- 1: Hydraulic Jack
- 2: Steel Column
- 3: Steel Assembly
- 4: Tens. /Comp. Load Cell
- 5: LVDT (300 mm)
- 6: LVDT (100 mm)
- 7: LVDT (25 mm)

10  
11  
12

**Fig. 3** Overview of WF-M in position ready for testing

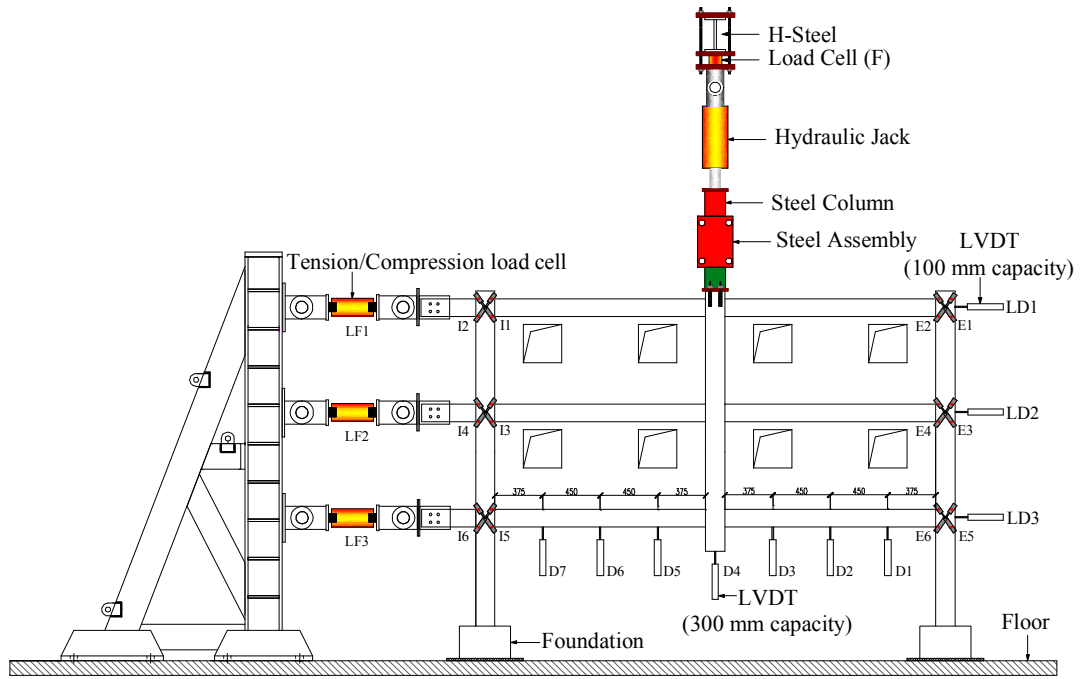


**Fig. 4** Schematic view of test setup and instrumentation layout

- 1
- 2
- 3
- 4
- 5

1  
2  
3  
4  
5  
6  
7  
8  
9  
10

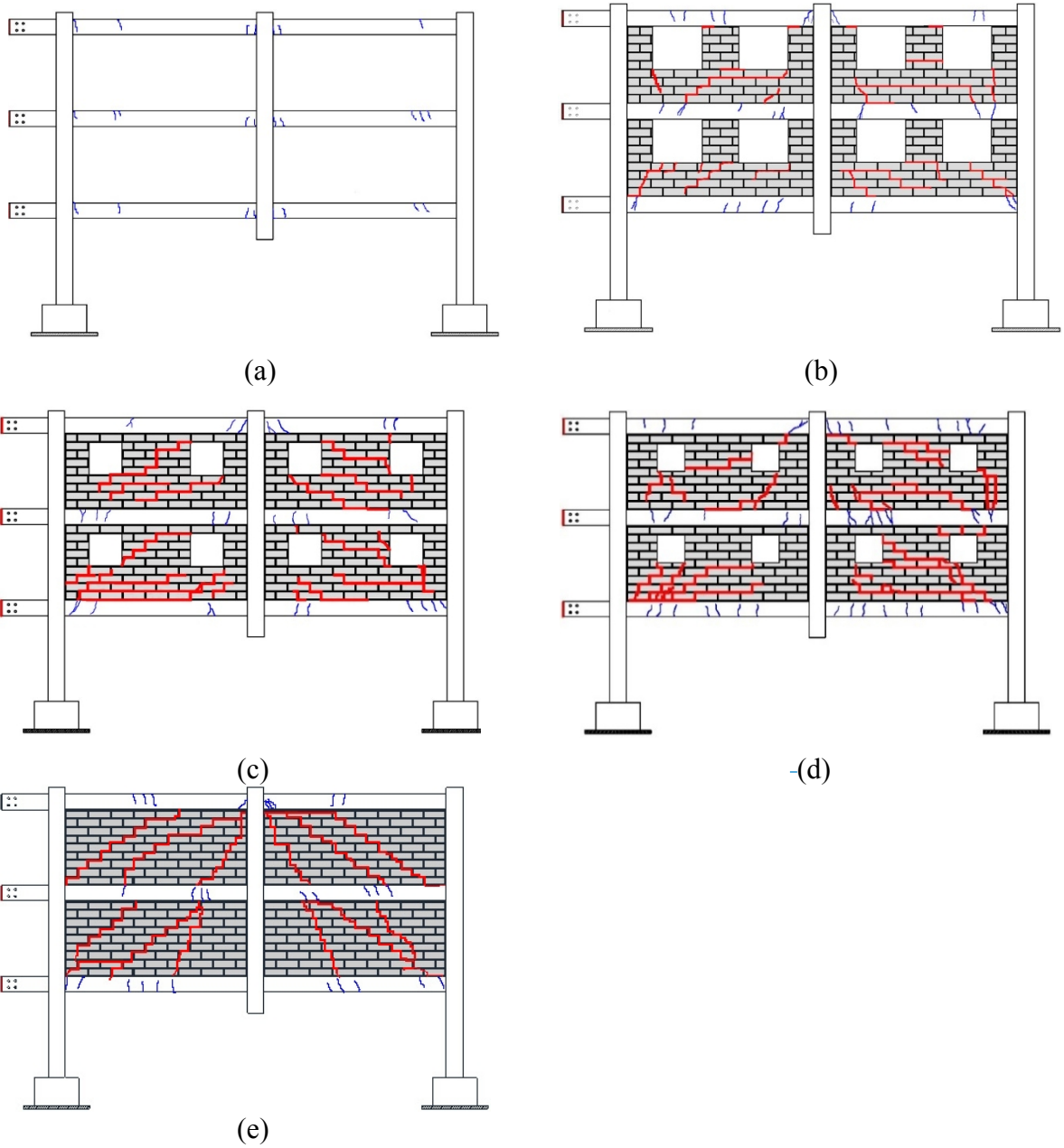
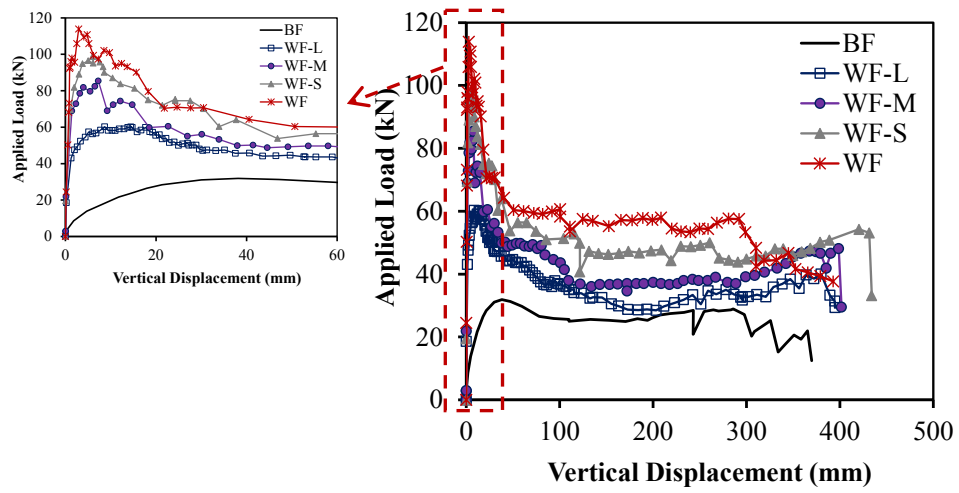


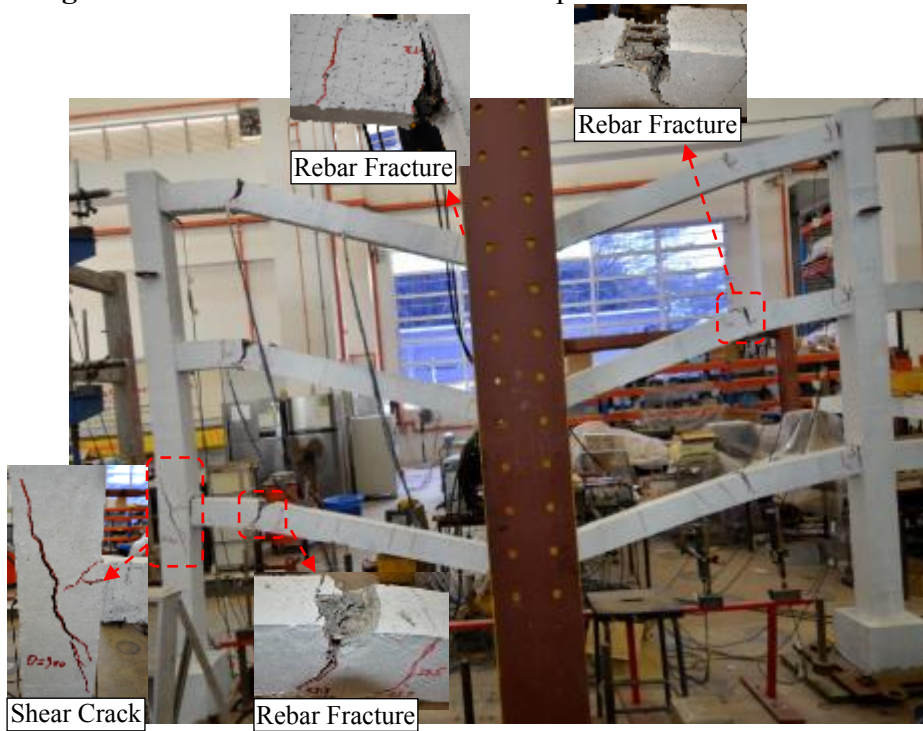
**Fig. 5** Crack pattern of the specimens at the CCD of 50 mm: (a) BF; (b) WF-L; (c) WF-M; (d) WF-S; (e) WF

1  
2  
3  
4



5  
6

**Fig. 6** Load resistance versus vertical displacement at center column



7  
8  
9  
10

**Fig. 7** Failure mode of BF

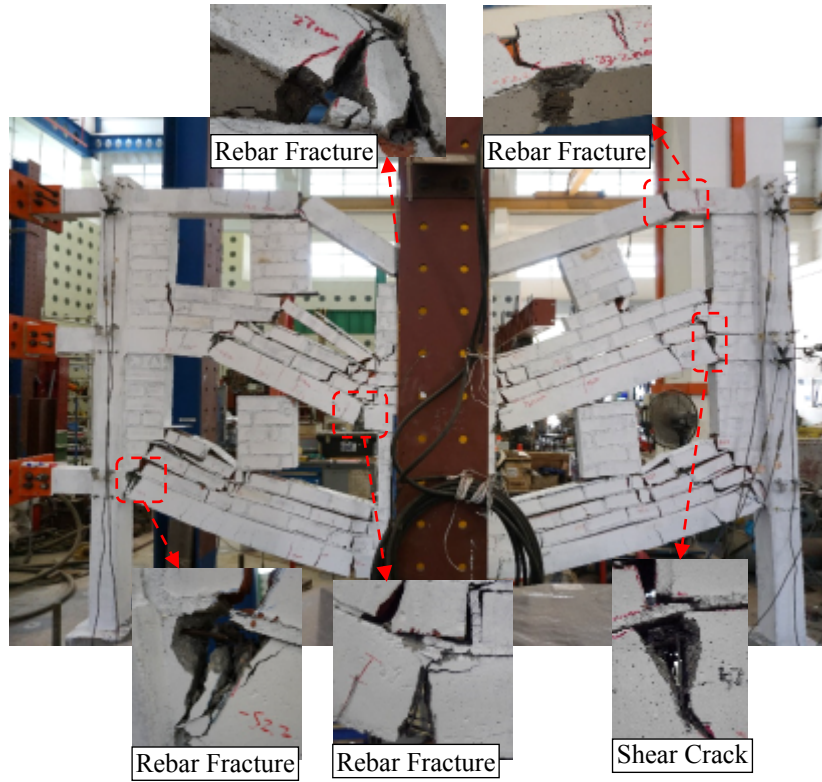


**Fig. 8** Failure mode of WF-L

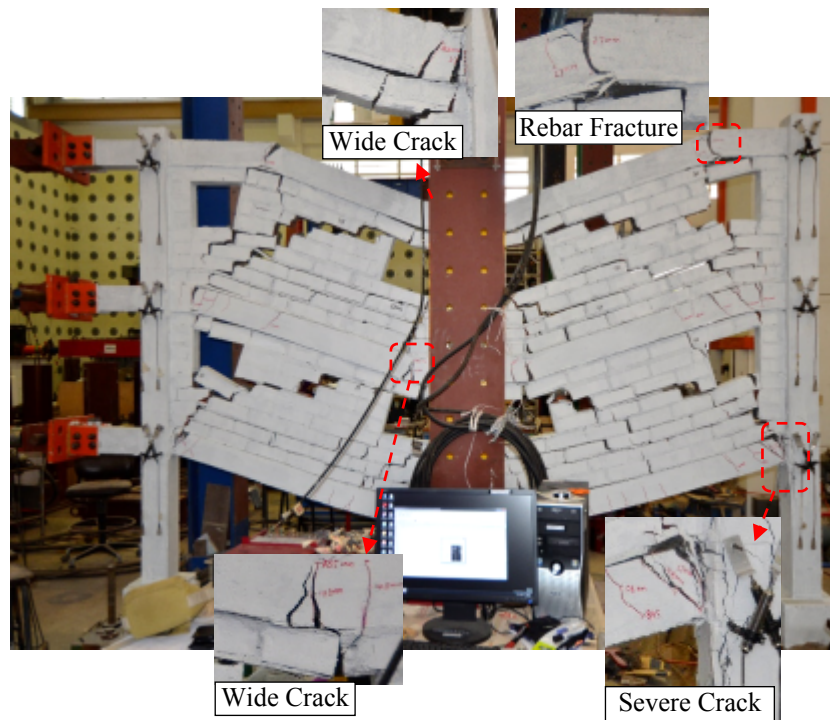


**Fig. 9** Failure mode of WF-M

1  
2  
3  
4

5  
6  
7  
8

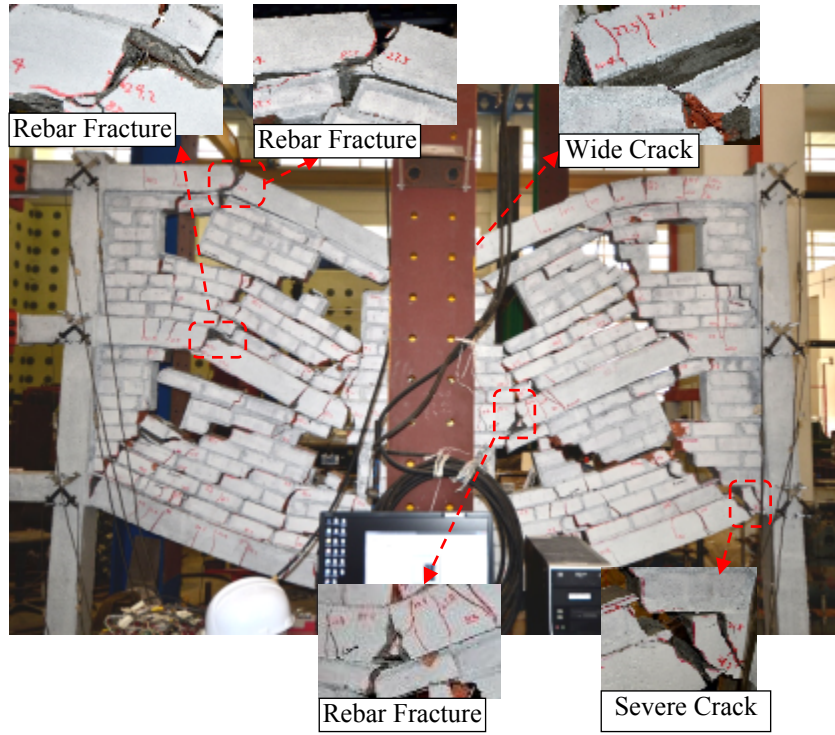


**Fig. 10** Failure mode of WF-S

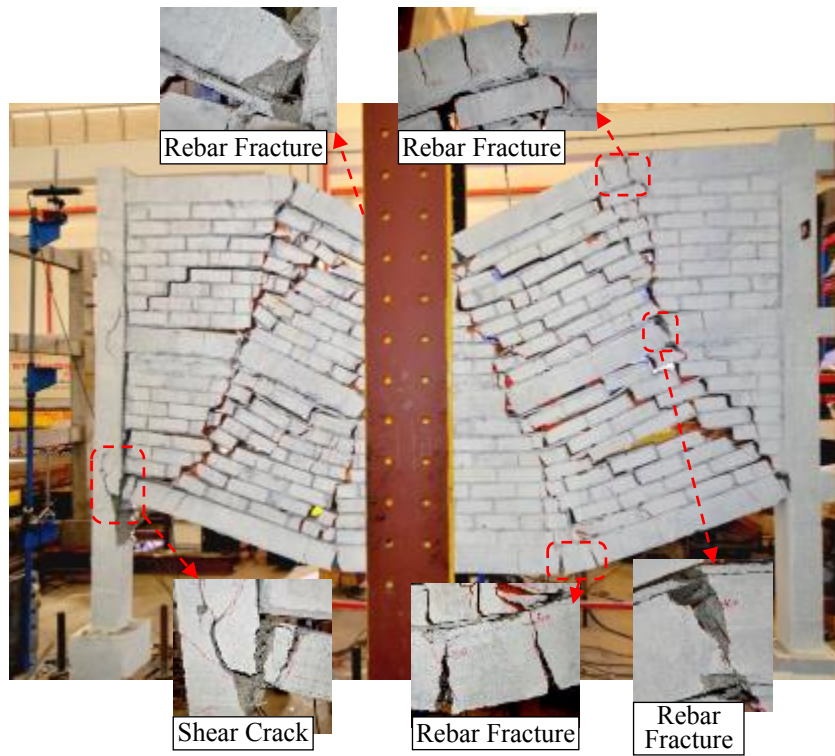


**Fig. 11** Failure mode of WF

1  
2  
3  
4

5  
6  
7  
8  
9  
10  
11

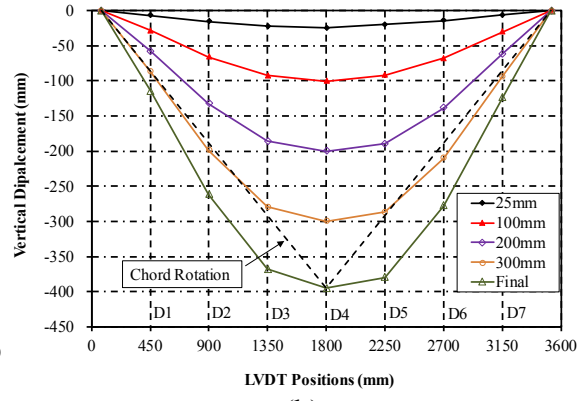
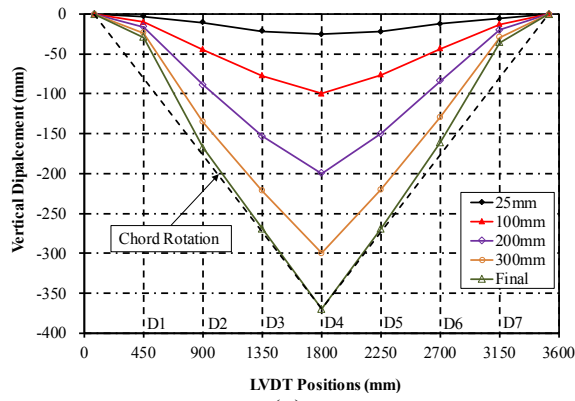


**Fig. 12** Overall deflection curve of beams in the first story: (a) BF; (b) WF-L

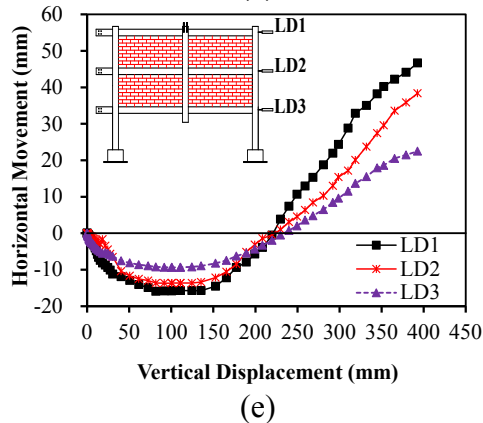
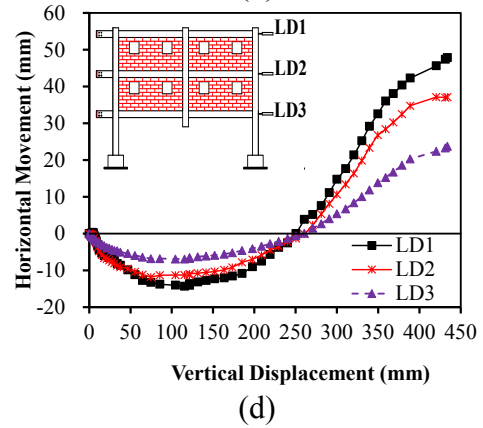
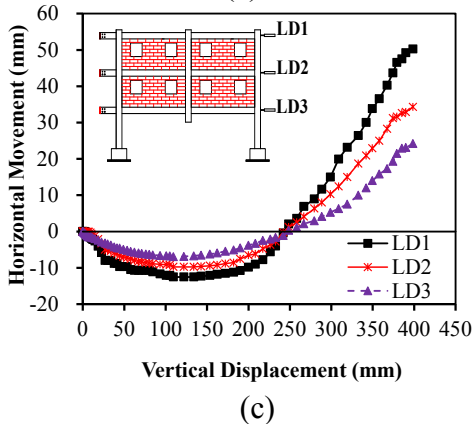
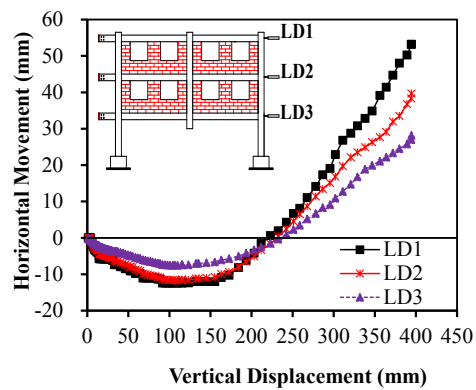
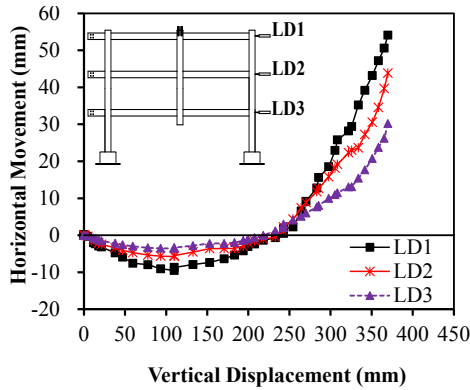
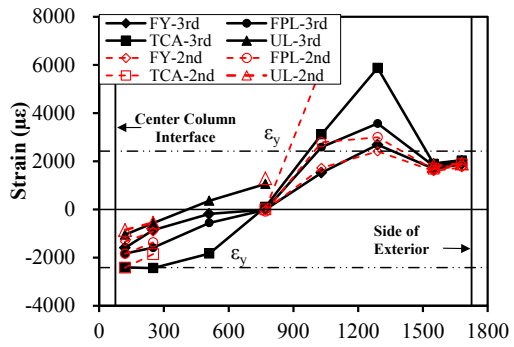
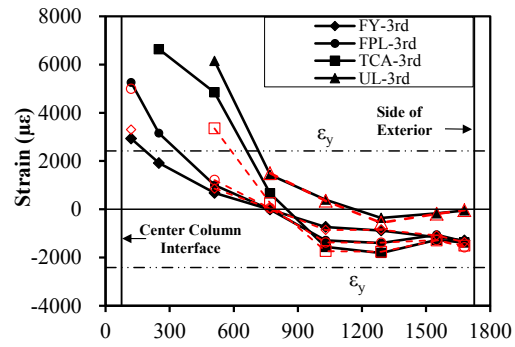


**Fig. 13** Horizontal movement of the exterior joints at different story: (a) BF; (b) WF-L, (c) WF-M; (d) WF-S; (e) WF



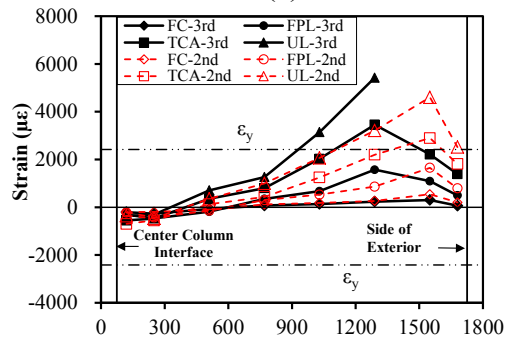
1 Distance from the adjacent column interface (mm)

2 (a)



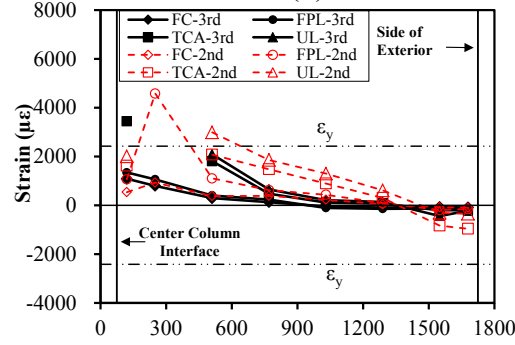
3 Distance from the adjacent column interface (mm)

4 (b)



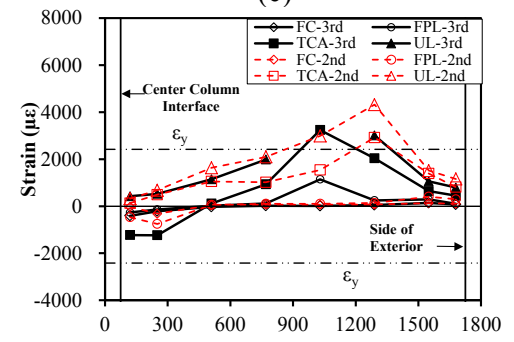
5 Distance from the adjacent column interface (mm)

6 (c)



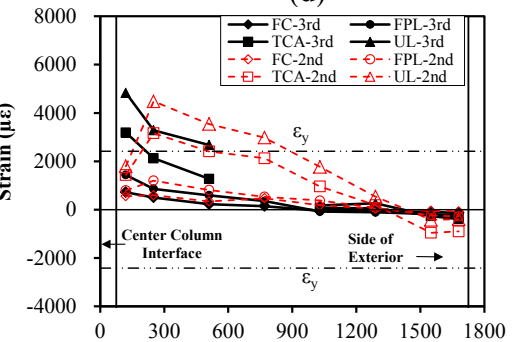
7 Distance from the adjacent column interface (mm)

8 (d)



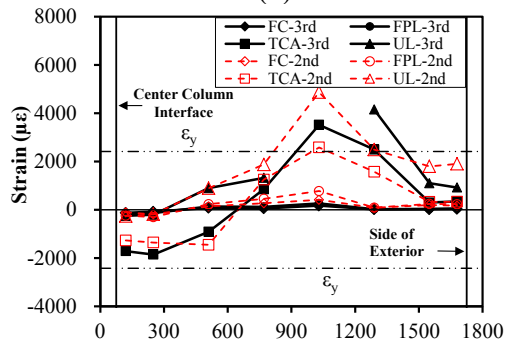
9 Distance from the adjacent column interface (mm)

10 (e)



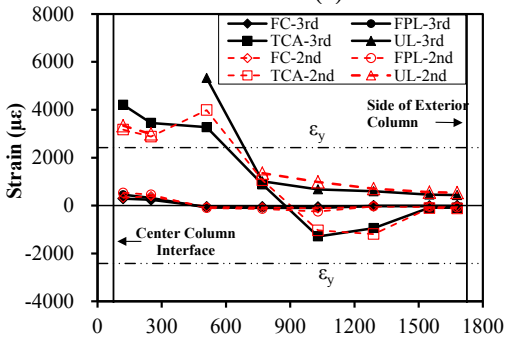
11 Distance from the adjacent column interface (mm)

12 (f)



13 Distance from the adjacent column interface (mm)

14 (g)



15 Distance from the adjacent column interface (mm)

16 (h)

**Fig. 14** Variation of strain results along the third floor beam longitudinal reinforcements: (a) top rebar in BF; (b) bottom rebar in BF; (c) top rebar in WF-L; (d) bottom rebar in WF-L; (e) top rebar in WF-S; (f) bottom rebar in WF-S; (g) top rebar in WF; (h) bottom rebar in WF

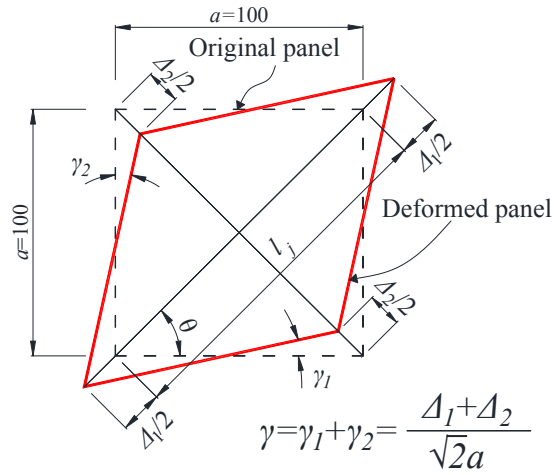


**Fig. 15** Method to determine the distortion of shear panel in joints

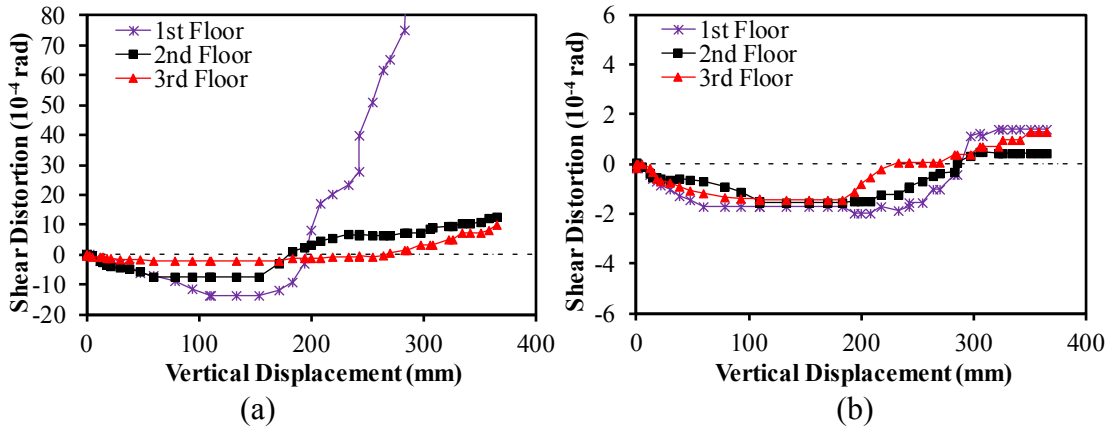


**Fig. 16** Variation of shear panel distortions of the joints in different stories of BF: (a) exterior joints, (b) interior joint

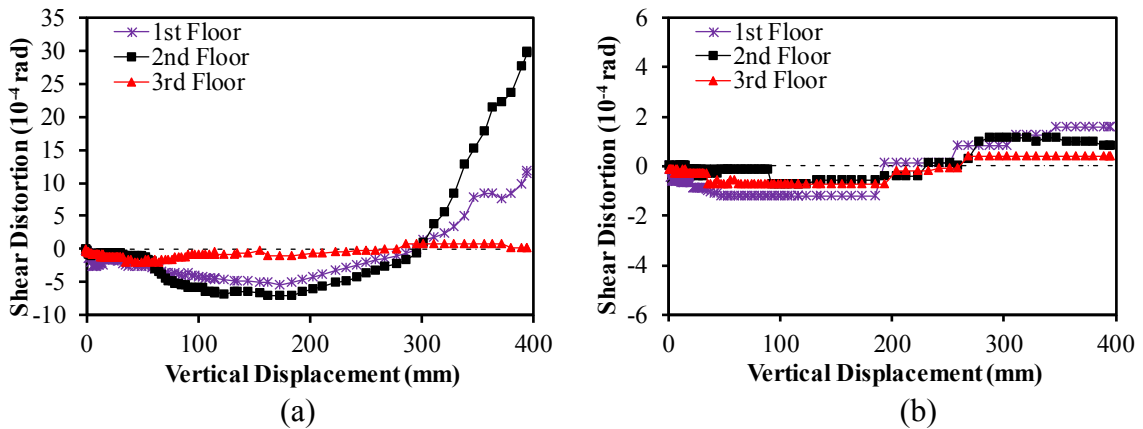


**Fig. 17** Variation of shear panel distortions of the joints in different stories of WF-L: (a) exterior joints, (b) interior joint

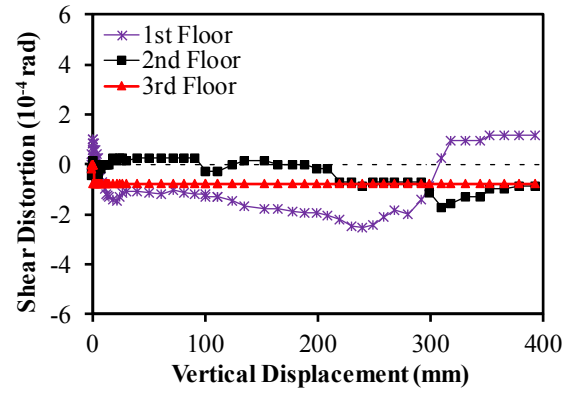
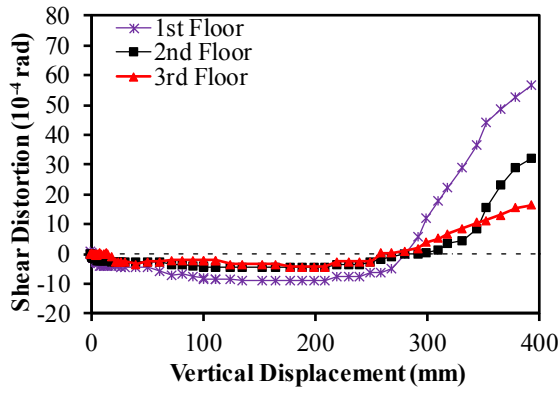


**Fig. 18** Variation of shear panel distortions of the joints in different stories of WF: (a) exterior joints, (b) interior joint

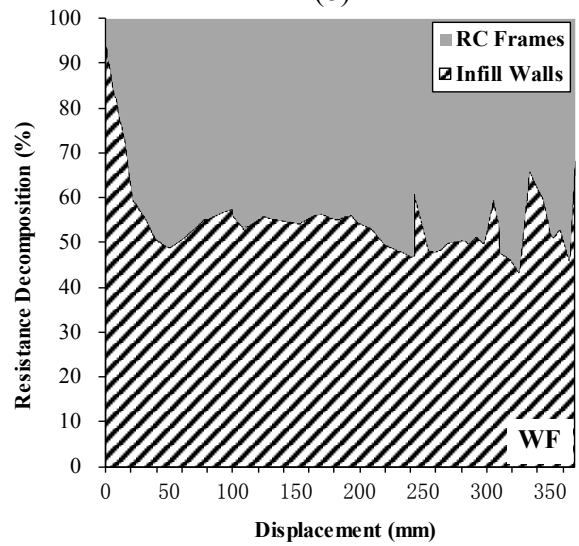
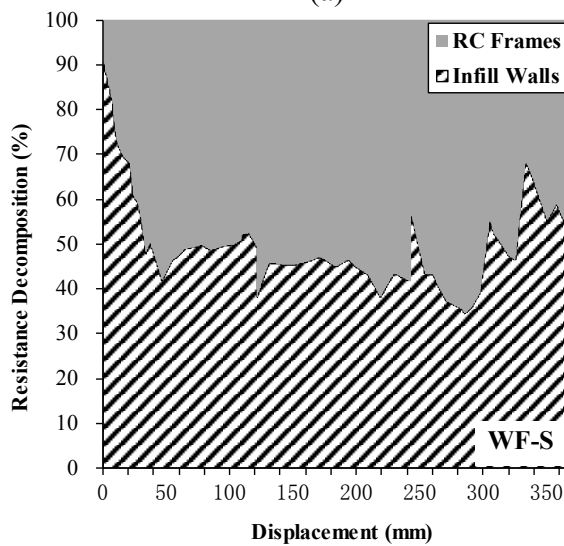
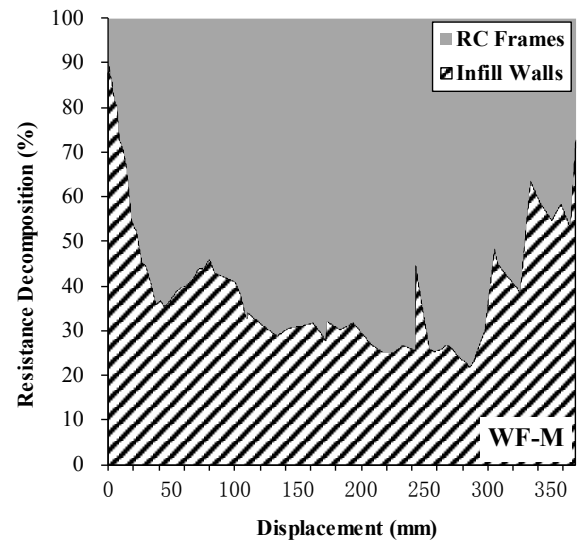
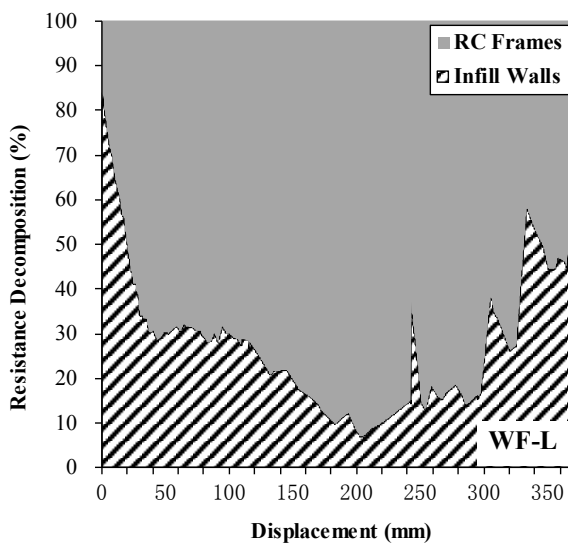
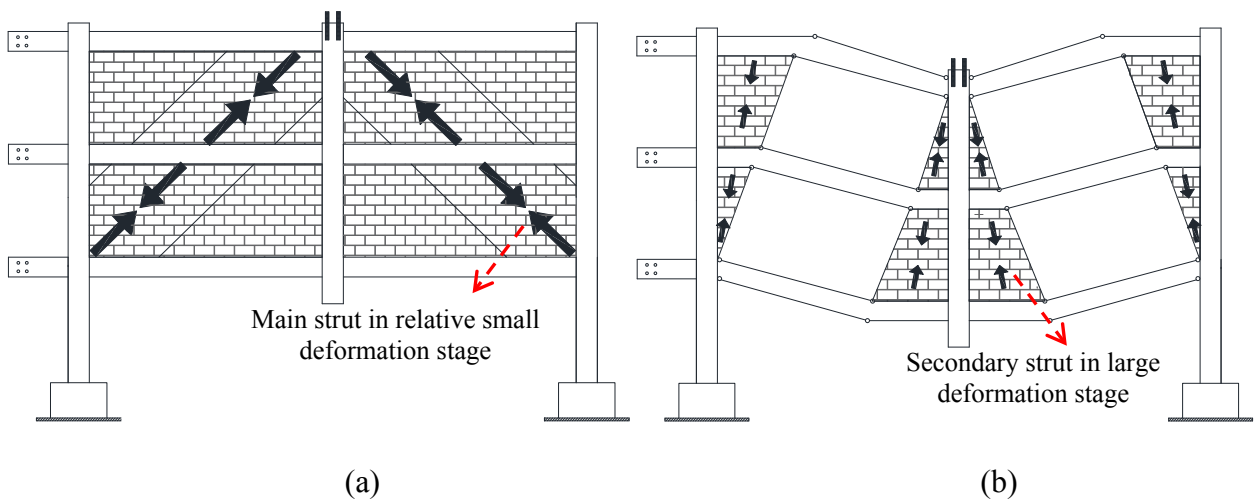


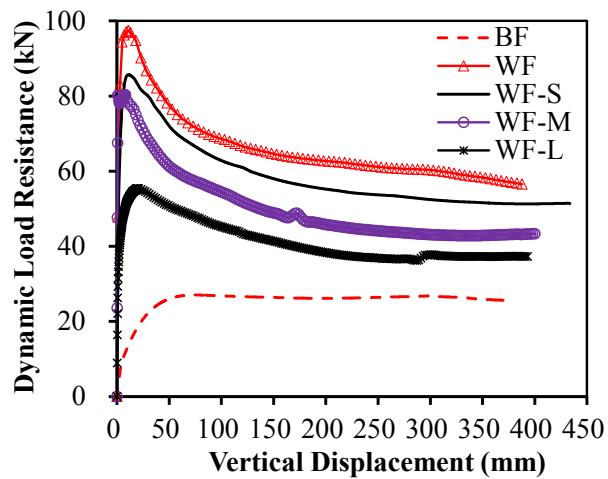
**Fig. 19** De-composition of the load resistance from RC frames and infill walls: (a) WF-L, (b) WF-M, (c) WF-S, and (d) WF

1  
2



3  
4  
5  
6  
7  
8  
9  
10  
11

**Fig. 20** Schematic view of equivalent compressive strut of infill walls: (a) at small deformation stage, (b) at large deformation stage



12  
13  
14  
15

**Fig. 21** Dynamic performance of the specimens